Coupling Substrate-Integrated Waveguides to Increase the Gain Bandwidth of Leaky-Wave Antennas

Citation for published version:
Poveda-García, M, Cañete-Rebenaque, D, Goussetis, G & Gómez-Tornero, JL 2018, 'Coupling Substrate-Integrated Waveguides to Increase the Gain Bandwidth of Leaky-Wave Antennas', *IEEE Transactions on Microwave Theory and Techniques*, vol. 66, no. 6, pp. 3099-3109.
https://doi.org/10.1109/TMTT.2018.2830396

Digital Object Identifier (DOI):
10.1109/TMTT.2018.2830396

Published In:
IEEE Transactions on Microwave Theory and Techniques

Coupling Substrate-Integrated Waveguides to Increase the Off-Broadside Scanned Gain Bandwidth of Leaky-Wave Antennas

Miguel Poveda-García, *Student Member IEEE*, David Cañete-Rebenaque, *Member IEEE*, George Goussetis, *Senior Member IEEE*, José Luis Gómez-Tornero, *Senior Member IEEE*.

Abstract—**A novel technique to increase the pattern bandwidth of directive off-broadside scanning substrate integrated waveguide leaky-wave antennas (SIW LWAs) is proposed. By shunt coupling several SIWs, it is shown that the gain at the desired scanning angle is kept stable in a wide frequency band. A systematic design methodology based on a simple transverse equivalent network is presented. Practical coupled-SIW designs with gain exceeding 10dB and scanning at 30º in the 15GHz band, are reported to validate the theory. Simulated and experimental results demonstrate an enhancement of the 3dB scanned pattern bandwidth from 2.5% (380 MHz) in the single-SIW design to 9% (1360 MHz) for a LWA composed of three coupled SIWs.**

Index Terms— **Leaky-wave antennas, frequency beam squint, broadband antennas, substrate integrated waveguide.**

I. Introduction

FREQUENCY-BEAM scanning is a well-known property of leaky-wave antennas (LWAs), intrinsic to the dispersive nature of leaky waves (LWs) [1]. It might be a useful characteristic for particular scenarios as frequency modulated-continuous wave (FMCW) radars [2]-[4], or frequency-steered near-field focusing systems [5]. However, the beam squint is an undesired feature which limits the practical instantaneous bandwidth in important applications as highly-directive point-to-point telecommunication radio links. For this reason, many efforts are recently put to design high-gain scanning LWAs with reduced frequency-scanning sensitivity [6]-[15]. Neto [6],[7] proposed a nondispersive printed leaky slot line embedded in a circularly symmetric elliptical dielectric lens which focus the radiated fields with high gain and fixed beam angle in a wideband. However, this solution lacks from the simple two-dimensional structure of planar LWAs. Planar LWAs using metamaterial unit-cells have been proposed to modify the frequency dispersion and reduce the beam squinting [8]-[11]. Anisotropic meta-substrates [12] and non-reciprocal ferrite-based metamaterials [13] have also proven beam squint reduction. Finally, active circuits can provide non-Foster dispersion responses for squint-free LWAs operating at an off-broadside scanning angle [14], [15]. In this paper we describe a totally different technique to reduce the off-broadside scanned gain bandwidth of planar LWAs in substrate integrated waveguide (SIW) technology, without the need of bulky dielectric lenses, metamaterial unit-cells, anisotropic materials, or active circuits. The novel structure is based on the SIW LWA [16] shown in Fig.1a, which is modified by adding extra longitudinally coupled SIWs ([17], [18]) as shown in Fig.1.

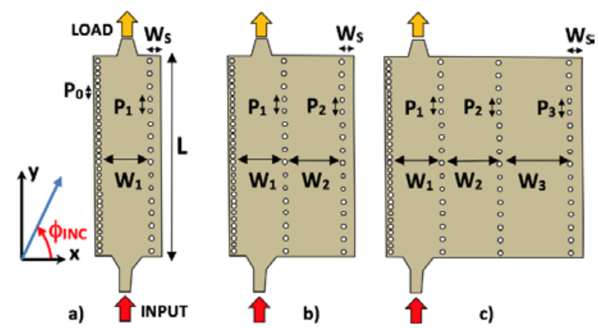

Fig. 1. Scheme of coupled SIW LWA of order a) N=1 b) N=2 c) N=3.

This coupled SIW LWA topology is inspired by a similar multi-layer arrangement used for Fabry-Pérot cavity antennas (FPA) [19]-[25]. The addition of extra coupled FP cavities has demonstrated increased pattern bandwidth for high-gain broadside radiation compared to the original single-cavity FPA. In the same manner, in this paper it is demonstrated for the first time that the high-gain scanned radiation pattern of the single SIW LWA (Fig.1a), can be improved in terms of gain bandwidth at a given off-broadside elevation angle by increasing the number of coupled SIWs. The design theory is based on a simple Transverse Equivalent Network (TEN) which is optimized to satisfy the associated phase resonance condition for the desired scanning angle over a wide band, as described in Section II. Practical examples of coupled SIW LWAs operating in the 15GHz band and scanning at a 30º angle are presented in Section III, illustrating that higher bandwidth with squint-free condition is obtained as the number N of coupled SIWs is increased from 1 to 3. Finally, Section IV reports experimental

Manuscript received October 5, 2017. This work has been supported by Spanish National project TEC2013-47037-C5-5-R, TEC2016-75934-C4-4-R, and Regional Seneca project 19494/PI/14.

M. Poveda-García, D. Cañete-Rebenaque and J.L. Gómez-Tornero are with the Group of Electromagnetism Applied to Telecommunications (GEAT), Technical University of Cartagena (UPCT), Cartagena 30202, Spain (e-mail: miguel.poveda@upct.es, david.canete@upct.es , josel.gomez@upct.es).

G. Goussetis is with the Institute of Sensors Signals and Systems, Heriot-Watt University, Edinburgh EH14 4AS, UK (e-mail: g.goussetis@hw.ac.uk)

validation performed on manufactured prototypes, and Section V presents the conclusions of this work.

II. Design Theory

The structure of the proposed coupled SIW LWA is illustrated in Fig.1. The original SIW LWA [16] shown in Fig.1a is formed by a single SIW of width W_1 created between a dense row of vias of diameter d and periodicity P_0 acting as totally reflective wall, and a partially reflective sheet (PRS) of vias with similar diameter d and located at a higher distance P_1 to allow for power leakage. A strip of width W_S produces radiation at its end fringe of length L located at the right side in Fig.1. A quasi-TE_{10} leaky mode with dispersive complex longitudinal propagation constant $k_y(f)$ can model this continuous radiation along the antenna length:

$$k_y(f) = \beta_y(f) - j\alpha_y(f) \tag{1}$$

The antenna length L behaves a magnetic-current line-source which radiates in the form of a scanned fan beam. The elevation scanning angle θ_R (measured from broadside, see Fig.2a) and the 3dB beamwidth $\Delta\theta$, are related to the leaky-mode phase constant β_y by the following equations:

$$\sin\theta_R(f) \approx \frac{\beta_y(f)}{k_0} = c_0 \frac{\beta_y(f)}{2\pi f} \tag{2}$$

$$\Delta\theta(f) \approx \frac{1}{\frac{L}{\lambda_0}\cos\theta_R(f)} \tag{3}$$

where k_0 is the free-space wavenumber, λ_0 is the free-space wavelength, and c_0 is the speed of light in air. To eliminate the frequency-beam squint, the scanning angle θ_R must be fixed to a constant goal value for all frequencies, so that from (2) we obtain a target linear dependence with frequency for $\beta_y(f)$:

$$\theta_R(f) = \theta_{GOAL} \rightarrow \beta_y(f) = \beta_{yGOAL}(f) = \frac{2\pi f}{c_0}\sin\theta_{GOAL} \tag{4}$$

To analyze the leaky-mode phase constant dispersion $\beta_y(f)$, a simple Transverse Equivalent Network (TEN) along the x-direction proposed in [26] and shown in Fig.2 can be used.

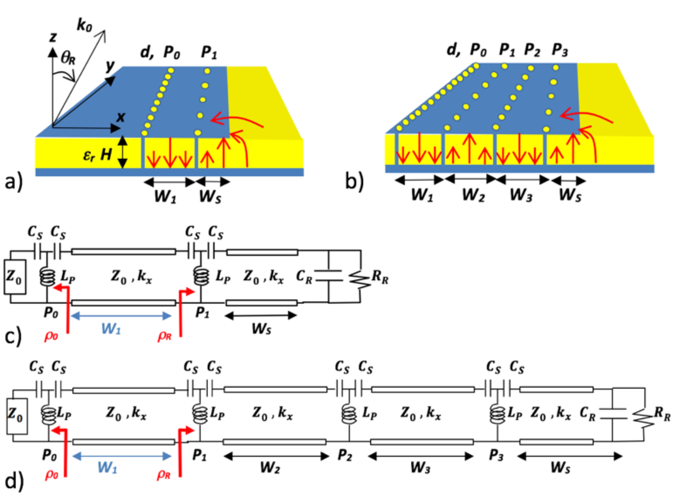

Fig. 2. 3D view of coupled-SIW LWA of order a) N=1 b) N=3 and associated Transverse Equivalent Network (TEN) c) N=1 d) N=3. Red lines in a) and b) represent the fundamental TE leaky-mode electric field distribution.

A T-junction network formed by two series capacitances C_S and a parallel inductance L_P given by Marcuvitz [27] is used to model each row of conducting vias of diameter d and for any periodicity P. The strip fringe radiation impedance is modeled by a shunt capacitor C_R and a shunt resistance R_R, which values are computed for the SIW host substrate of height H and relative dielectric constant ε_r using Kuester approximation for thin substrates [28]. It must be taken into account that the values for C_S, L_P, C_R and R_R depend on the internal angle of incidence ϕ_{INC} shown in Fig.1a [26], which is related to the leaky radiation angle θ_R and phase constant β_y by the Snell equation:

$$\sin\varphi_{INC}(f) = \frac{\sin\theta_R(f)}{\sqrt{\varepsilon_r}} \approx \frac{\beta_y(f)}{k_0\sqrt{\varepsilon_r}} \tag{5}$$

For the efficient design of the multi-cavity SIW LWA, the values of C_S, L_P are first computed for a range of posts periodicity values P using an accurate home-made analysis code based on the Method of Moments (MoM) [26], and for any fixed incidence angle ϕ_{INC}. Then a second-grade polynomial fitting is carried out to obtain closed-form expressions for the component values as a function of P:

$$L_P(P) = a_L P^2 + b_L P + c_L \tag{6}$$

$$C_S(P) = a_C P^2 + b_C P + c_C \tag{7}$$

Figure 3 represents these functions for an internal angle of incidence ϕ_{INC}=19º, as a function of P in the range from P= 2 mm to P=7 mm, and for a post diameter d=1 mm. They are compared with MoM results showing good agreement in the full range of values of P. Clearly the use of closed-form analytical expressions lower the computational cost needed compared to full-wave MoM analysis. This time reduction is indispensable for the subsequent optimization technique, which needs hundreds of analyses to properly design the distance P between coupling posts for each row of coupling vias.

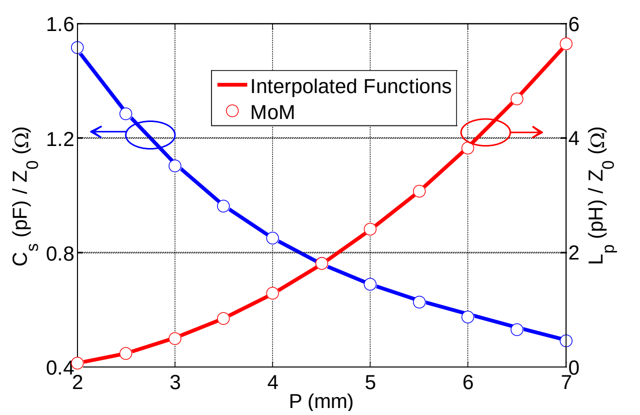

Fig. 3. Variation of the C_S and L_P as a function of vias periodicity P and frequency for a fixed incidence angle ϕ_{INC}=19º, with d=1mm.

Finally, the SIWs are modelled in the TEN by transmission lines of length W_i, TE characteristic impedance $Z_0=1/\omega k_x$ and complex transverse propagation constant $k_x(f)$ related to the leaky-mode longitudinal constant $k_y(f)$ (1) by:

$$k_x(f) = \sqrt{{k_0}^2\varepsilon_r - k_y(f)^2} = \beta_x(f) + j\alpha_x(f) \tag{8}$$

Under low-leakage conditions ($\alpha_y << \beta_y$) and using (2), (8) can be rewritten as a function of frequency and the scanning angle θ_R:

$$k_x(f) \approx \beta_x(f) = \frac{2\pi f}{c_0}\sqrt{\varepsilon_r - sin^2\theta_R(f)} \qquad (9)$$

so that the transverse phase constant $\beta_x(f)$ must follow the next linear function with frequency to satisfy the squint-free goal condition (4):

$$\beta_{xGOAL}(f) = \frac{2\pi f}{c_0}\sqrt{\varepsilon_r - sin^2\theta_{GOAL}} \qquad (10)$$

The leaky-mode dispersion is given by the Transverse Resonance Equation (TRE):

$$\rho_0 e^{-j2k_x W_1}\rho_R = 1 \qquad (11)$$

where ρ_R and ρ_0 stand for the reflection coefficients at the right and left sides of the SIW of width W_1 (see Fig.2). Inserting (10) in (11) and taking phases, the following goal function $\Psi_{GOAL}(f)$ is obtained for the phase of the reflection coefficient ρ_R, as a function of frequency and for the goal scanning angle θ_{GOAL} , and a given width W_1:

$$\Psi_{GOAL}(f) = \frac{4W_1\pi f}{c_o}\sqrt{\varepsilon_r - sin^2\theta_{GOAL}} - \varphi_0(f,\varphi_{GOAL}) + 2\pi q \qquad (12)$$

where q is any integer value, and φ_0 is the phase of ρ_0 which depends on frequency and on the internal incidence angle ϕ_{INC}. As for the radiation scanning angle θ_R, the internal angle of incidence ϕ_{INC} is also fixed to a goal value to keep the squint-free condition. Inserting (4) in (5) we obtain:

$$\varphi_{INC}(f) = \varphi_{GOAL} = asin\frac{sin\theta_{GOAL}}{\sqrt{\varepsilon_r}} \qquad (13)$$

The design goal is thus to determine the coupled SIWs cross section dimension (distances between coupling vias P_i, and SIW widths W_i) which satisfy over a wideband the reflection-phase condition $\Psi_R(f)=\Psi_{GOAL}(f)$, or in other words, which minimize the following error function for the reflection phases:

$$\Delta\Psi(f, W_i, P_i) = \Psi_{GOAL}(f, W_1) - \Psi_R(f, W_{i>1}, P_i) \qquad (14)$$

where it has been highlighted that the first SIW width W_1 determines the goal reflection phase Ψ_{GOAL}, while the rest of SIW widths W_i with i>1 and the distance between coupling vias P_i, determine the reflection phase of the right part of the circuit Ψ_R. The design methodology is described in the next section with practical examples.

III. Design Examples

The SIW substrate is set to H=0.508 mm, ε_r=2.2, and the diameter of the vias is fixed to d=1 mm. The row of vias at the left is set to a distance P_0=2 mm so that leakage is prevented from this side. The desired scanning angle is chosen to θ_{GOAL}=30º and the design frequency is 15 GHz. The internal incidence angle (13) is then fixed to ϕ_{GOAL}=19º. The following subsections illustrate how an increased number of coupled SIWs (from N=1 to N=3) can be optimized to provide higher squint-free bandwidth. Table I summarizes the optimized dimensions of the five studied designs.

Table I. Optimized Dimensions of Coupled SIW LWA for θ_{GOAL}=30º

N	SIW Width W_i (mm)	Vias Periodicity P_i (mm)
1	W_1=7.45 W_S=1.8	P_1=3.6
2a	W_1=7.37 W_2=8.27 W_S=2.52	P_1=3.76 P_2=7.75
2b	W_1=7.29 W_2=7.98 W_S=2.58	P_1=3.91 P_2=7.75
2c	W_1=7.23 W_2=7.88 W_S=2.58	P_1=4.06 P_2=7.75
3	W_1=7.19 W_2=6.93 W_3=6.9 W_S=2.99	P_1=3.57 P_2=3.29 P_3=3.37

A. Single SIW LWA (N=1)

For the single SIW LWA, the dimensions W_1, P_1 and W_S, can be directly obtained as explained in [26] to satisfy the scanning angle at the desired frequency (θ_{GOAL}=30º at 15GHz), obtaining the values summarized in Table I for N=1. With these dimensions, Fig.4 shows the goal reflection-phase $\Psi_{GOAL}(f)$ for a squint-free response in the frequency band from 12GHz to 18GHz. Also, the magnitude $|\rho_R(f)|$ and the phase $\Psi_R(f)$ of the reflection coefficient ρ_R for this N=1 design are plotted. As shown in Fig.4, the reflection-phase condition $\Psi_R(f)=\Psi_{GOAL}(f)$ for leaky-mode radiation at fixed θ_R=30º is only satisfied at the design frequency of 15 GHz. The goal reflection phase $\Psi_{GOAL}(f)$ has a positive slope with frequency, which cannot be followed by the reflection phase $\Psi_R(f)$ of a single row of PRS posts, which has a negative phase gradient as shown in Fig.4.

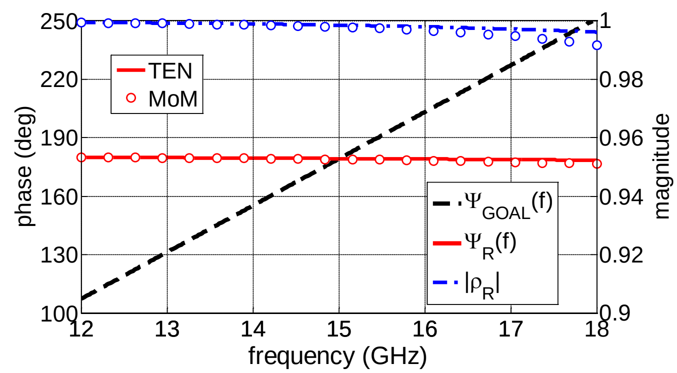

Fig. 4. Reflection coefficient for single-cavity SIW LWA with dimensions given in Table I with N=1, and reflection-phase goal function for θ_{GOAL}=30º.

The frequency response for the directivity of this N=1 SIW LWA design has been simulated using HFSS software [29] for a finite antenna of length L=16cm (L=8λ_0 at 15GHz). Figure 5 represents the directivity frequency response obtained at the desired scanning angle $\theta=\theta_{GOAL}$=30º in the frequency range from 14GHz to 16GHz. Due to the inherent frequency-scanning behavior of LWAs [1], a narrow beam with $\Delta\theta$=8º (3) is scanned from near-broadside (θ=0º) at low frequencies to endfire (θ=90º) direction as frequency is increased. The maximum of directivity at the desired scanning angle $\theta=\theta_{GOAL}$=30º is observed at the design frequency of 15GHz.

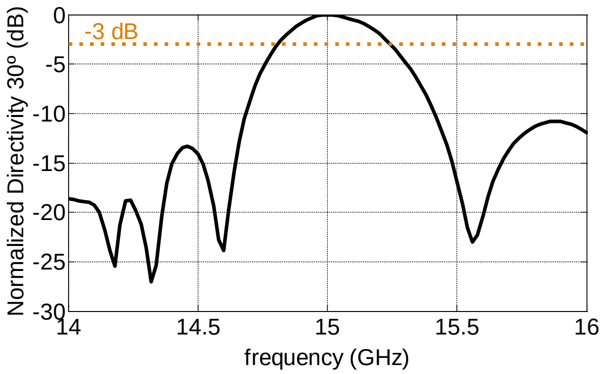

Fig. 5. Normalized directivity at $\theta=\theta_{GOAL}$=30º as a function of frequency for the N=1 SIW LWA with dimensions given in Table I.

The directivity at 30º drops above and below this design frequency of 15 GHz, resulting in a 3dB *scanned pattern bandwidth* (SPBW) of 430MHz, as illustrated in Fig.5. Longer LWA provide narrower scanned beams (3) and higher directivities and thus reduced SPBW, while shorter antennas result in wider beams and higher bandwidth. In any case, this is the common behavior of LWAs, which limits its performance for broadband point-to-point applications as commented in the introduction of this paper.

B. Two coupled SIW LWA (N=2)

Broadband operation with a fixed scanning angle can be obtained if the antenna reflection phase response $\Psi_R(f)$ provides a positive phase gradient which matches $\Psi_{GOAL}(f)$ in the desired bandwidth. Similar positive phase-gradient responses have been applied for wideband FPA radiating at broadside [19]-[25], [30]-[33]. In our case, this type of response can be obtained by inserting an extra row of vias with period P_2 which couples energy to an extra SIW of width W_2, thus leading to a coupled SIW LWA of order N=2 as represented in Fig.1b.

This is illustrated in Fig.6, where the reflection coefficients (magnitude and phase) for three different coupled SIW LWA designs with N=2 are plotted. The coupled SIW dimensions were optimized to minimize the phase-error function (14) as explained in Section II, and they are summarized in Table I. As can be observed, the reflection phase $\Psi_R(f)$ now presents a positive slope which satisfies the squint-free condition $\Psi_R(f)=\Psi_{GOAL}(f)$ for θ_{GOAL}=30º not only at 15GHz, but in given bandwidth starting at 15GHz and ending at 15.31 GHz for case N=2a (Fig.6a), 15.52 GHz for case N=2b (Fig.6b), and 15.65 GHz for case N=2c (Fig.6c). Also, the reflection magnitude $|\rho_R(f)|$ is different to the N=1 case, showing a resonant behavior around the design frequency of 15GHz.

The resulting phase-error functions $\Delta\Psi(f)$ (14) for these three designs are plotted in detail in Fig.7. It can be observed that the squint-free condition $\Delta\Psi(f)$=0 is satisfied at 15GHz, and also at two extra frequency points above, which can be distributed closer or further apart to determine the resulting free-squint bandwidth. The case N=2a in Fig.7 shows a squint-free range from 15 GHz to 15.31 GHz, the case N=2b from 15 GHz to 15.52 GHz, and the case N=2c from 15 GHz to 15.65 GHz.

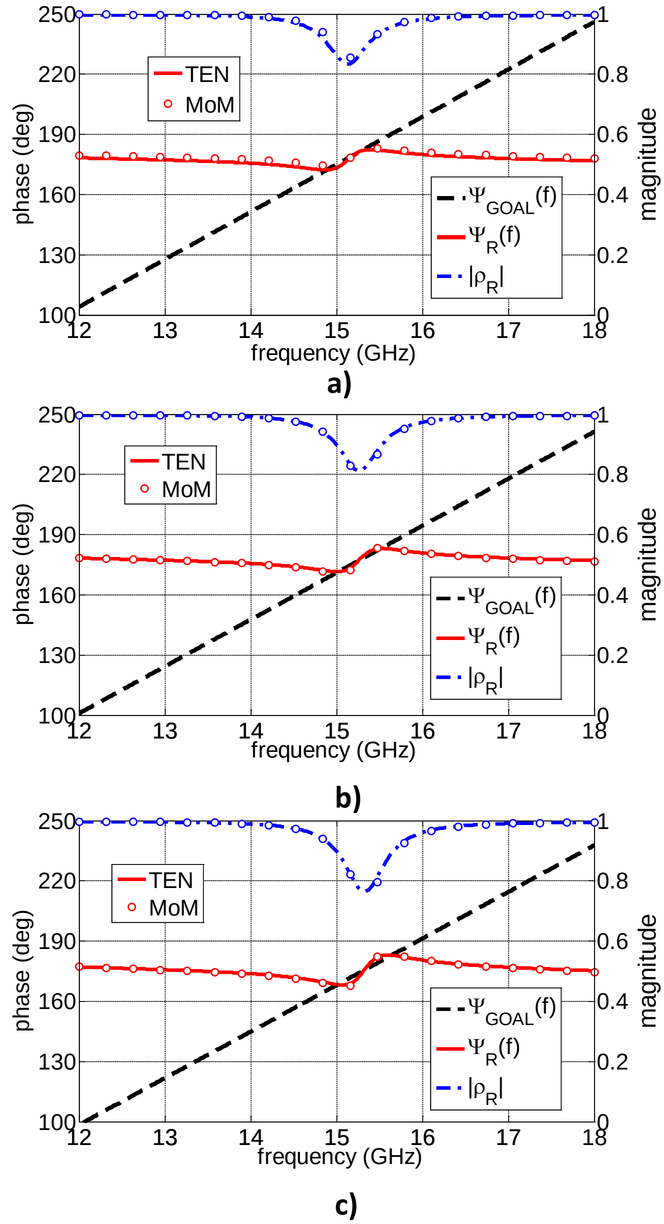

Fig. 6. Reflection coefficient for optimized coupled SIW LWA with N=2 and dimensions given in Table I, and reflection-phase goal function for θ_{GOAL}=30º.

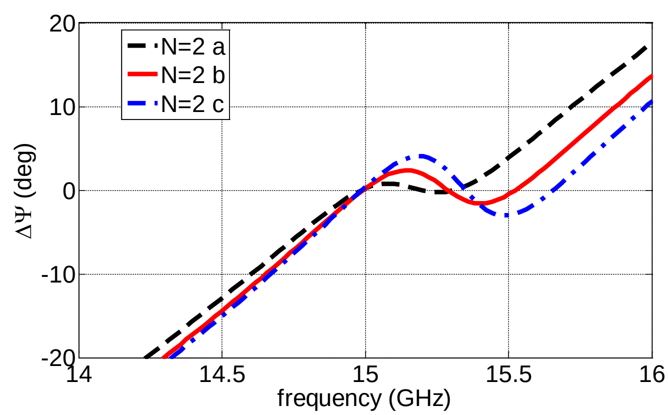

Fig. 7. Reflection-phase error function (with scanning angle θ_{GOAL}=30º) for optimized coupled SIW LWA designs of Table I with N=2.

Although one could think that more separated squint-free frequency points provide a wider free-squint bandwidth, this is not strictly true. Actually, the condition $\theta_R=\theta_{GOAL}=30^o$ is guaranteed only at the 2N-1 frequency points where the TEN reflection-phase error function $\Delta\Psi(f)$ is zero. As shown in Fig.7, intermediate frequency points provide higher phase error as the frequency zeros are more separated (see N=2c in Fig.7). On the contrary, closer zeroes provide a flatter response of the error function (see N=2a in Fig.7). As the error function $\Delta\Psi(f)$ becomes higher, the condition $\theta_R=\theta_{GOAL}=30^o$ is less certain and it is expected the associated leaky-mode scanning angle θ_R to be more distant from the desired angle of 30º.

To obtain the variation with frequency of the leaky-mode scanning angle $\theta_R(f)$ w.r.t to the desired fixed angle θ_{GOAL}, a leaky-mode dispersion analysis must be carried out. An approximate dispersion analysis can be performed by inserting in (11) the complex reflection coefficient $\rho_R(f)$ obtained for the optimized designs (shown in Fig.6). Then, the TRE (11) is solved for the unknown complex transverse propagation constant $k_x(f)$, from which the leaky-mode longitudinal propagation constant $k_y(f)$ can be derived using (8). Finally, from the phase constant $\beta_y(f)$, the dispersion with frequency of the scanning angle $\theta_R(f)$ is obtained using (2).

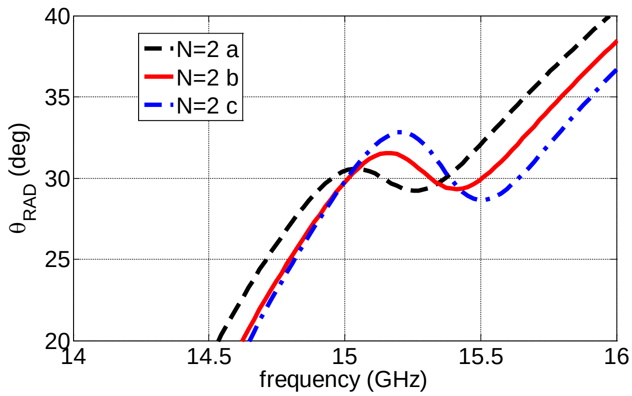

Fig 8. Dispersion of the leaky-mode scanning angle for optimized coupled SIW LWA designs of Table I with N=2.

Figure 8 shows the frequency dispersion for $\theta_R(f)$ for the three SIW LWAs designs of order N=2. As expected, the three designs satisfy the condition $\theta_R=\theta_{GOAL}=30^o$ at 15GHz and at two more frequency points which correspond with the frequencies of zero phase-error in Fig.7. For intermediate frequencies, the leaky-mode scanning angle fluctuates from the goal angle of 30º, being this deviation more pronounced for case N=2c (30º ± 2.8º), and less pronounced for case N=2a (30º ± 1.5º).

Since the objective is to keep the LWA scanning angle as fixed as possible to the desired angle $\theta_R=\theta_{GOAL}=30^o$ and over the wider band, there is a trade-off in the location of the frequency zeros of $\Delta\Psi(f)$. The ultimate result which determines the optimum design is the frequency response of the antenna directivity at the desired off-broadside scanning direction (30º in our case). This is obtained with HFSS and plotted in Fig.9 for the three designs of order N=2 (all of them with the same antenna length than for the N=1 design, i.e. L=16cm).

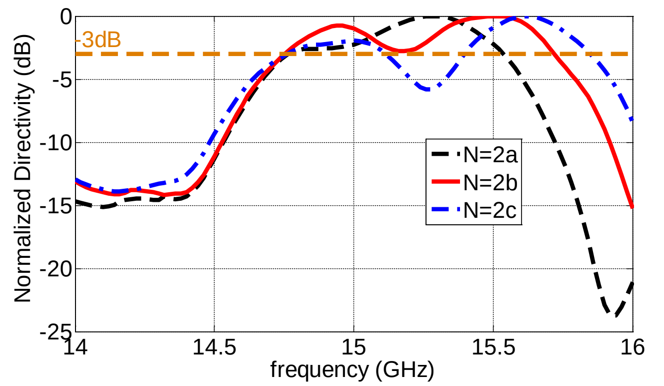

Fig. 9. Normalized directivity at $\theta=\theta_{GOAL}=30^o$ as a function of frequency for optimized coupled SIW LWA designs of Table I with N=2.

For the case N=2a, a 3dB SPBW from 14.75GHz to 15.53GHz (780MHz) is obtained, showing slight improvement when compared to the N=1 case with 430MHz of SPBW (see Fig.5). This can be attributed to the too close location of the squint-free frequency points in Fig.8. On the contrary, the case N=2c showed too separated frequency zeros and too strong variation in the leaky-mode scanning angle (see Fig.8), which results in a strong drop of directivity for intermediate frequency points as observed in Fig.9 around 15.25GHz. Therefore, the optimum design corresponds to the case N=2b, which provides a more stable directivity response, offering a SPBW of 970MHz from 14.75GHz to 15.72GHz.

As previously commented, this numerical optimization is affordable thanks to the use of closed-form expressions for all the components of the TEN. A gradient-based optimization scheme has been used to minimize the error function (12), taking 1500 simulations for convergence. To validate the results, the reflection coefficient $\rho_R(f)$ obtained with MoM is also represented with circles in Fig.6, showing good agreement.

C. Three coupled SIW LWA (N=3)

Following a similar optimization procedure than for the N=2 SIW LWA, a third-order (N=3) SIW LWA has been designed using the TEN shown in Fig.2d. The optimized dimensions are summarized in Table I, and the resulting reflection coefficient is plotted in Fig.10. Again, good matching is observed between TEN and full-wave MoM results for this N=3 design.

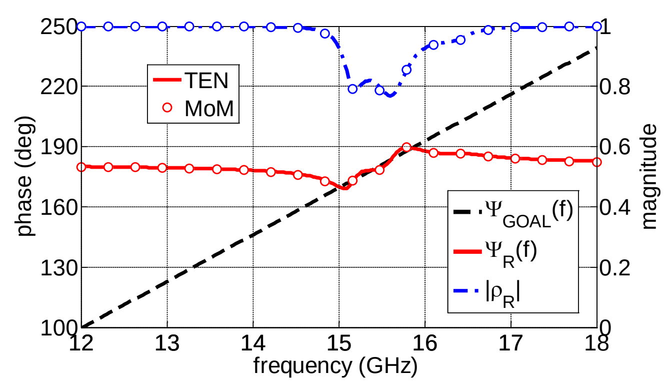

Fig. 10. Reflection coefficient for optimized coupled SIW LWA with N=3 and dimensions given in Table I, and reflection-phase goal function for $\theta_{GOAL}=30^o$.

Figure 11 compares the phase-error function of this N=3 design, with the error functions obtained for N=1 and N=2b. As expected, the squint-free condition $\Delta\Psi(f)=0$ is satisfied at 2N-1=5 frequency points which can be distributed in a wider bandwidth (from 15GHz to 15.85GHz) than for the N=1 and N=2 cases.

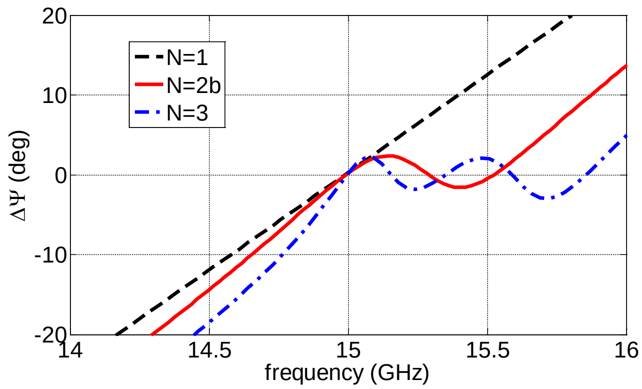

Fig. 11. Reflection-phase error function (with scanning angle θ_{GOAL}=30º) for optimized coupled SIW LWA designs of Table I with N=1, N=2b and N=3.

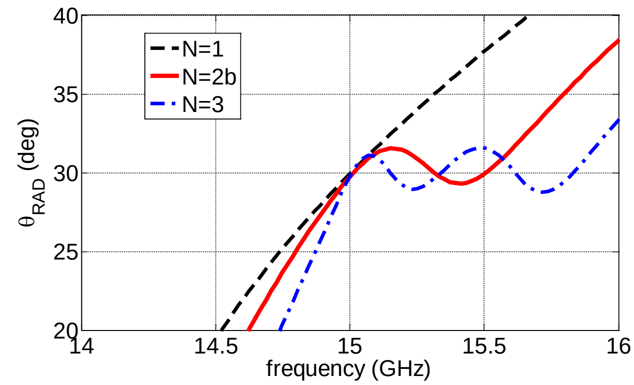

Fig. 12. Dispersion of the leaky-mode scanning angle for optimized coupled SIW LWA designs of Table I with N=1, N=2b and N=3.

Figure 12 compares the leaky-mode angle dispersion $\theta_R(f)$. The single SIW LWA (N=1) shows a conventional leaky-mode dispersion [1], [5], with a scanning angle which monotonously rises with frequency. Therefore, the condition θ_R=θ_{GOAL}=30º can only be satisfied at one frequency point (15GHz). However, the coupled SIW designs (with N>1) present a frequency band with anomalous quasi-oscillatory stabilization of $\theta_R(f)$ around the desired off-broadside scanning angle. This type of oscillatory anomalous leaky-mode dispersion was reported in [33] for a multilayer broadband FPA radiating at broadside; this is the first time it is demonstrated for a LWA scanning off-broadside.

In our case, the leaky-mode scanning angle $\theta_R(f)$ oscillates around θ_{GOAL}=30º, as shown in Fig.12. As for the N=2b case, the ripples of $\theta_R(f)$ have been kept within a level of 30º±1.5º, so that the SPBW is optimized as explained in subsection III.B. The case N=3 presents 5 frequency points which satisfy θ_R=θ_{GOAL}=30º, and which are distributed in the aforementioned squint-free bandwidth from 15 GHz to 15.85 GHz (850MHz). This is an improvement compared to the N=2b design that shows a squint-free bandwidth from 15 GHz to 15.52 GHz (520MHz).

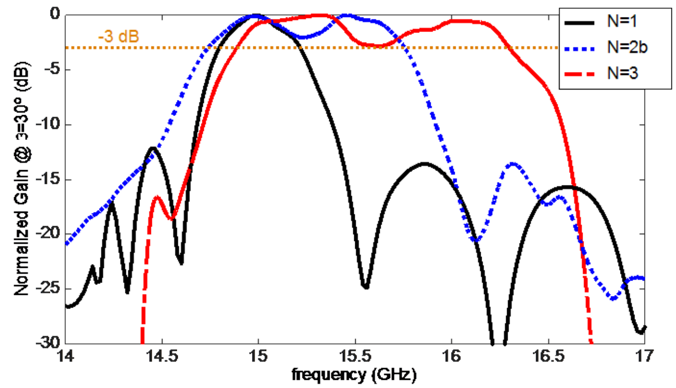

Fig. 13. Normalized gain at θ=θ_{GOAL}=30º as a function of frequency for optimized coupled-SIW LWA designs of Table I with N=1, N=2b and N=3.

TABLE II. 3DB GAIN BANDWIDTH FOR DESIGNS IN TABLE I

Case	half-power gain bandwidth at θ=30º	SPBW at θ=30º	Fractional BW
N=1	14.81 GHz – 15.24 GHz	400 MHz	2.6 %
N=2b	14.75 GHz – 15.72 GHz	970 MHz	6.4 %
N=3	14.88 GHz – 16.30 GHz	1420 MHz	9.5 %

Finally, Fig.13 shows the normalized gain at 30º obtained with HFSS, for the three optimized designs with N=1, N=2b and N=3. These full-wave results demonstrate how the gain at 30º presents a bandpass frequency response which half-power gain bandwidth increases with the number of coupled SIWs. Particularly, the low frequency limit in Fig.13 is close to 14.5 GHz, which corresponds to the onset of the leaky mode in the coupled SIW structure for the three designs. Then, the gain rises and oscillates with low ripple (below 3dB), and above a given upper frequency it drops. This behavior is in coherence with the leaky-mode dispersion curves in Fig.12. Table II summarizes the half-power gain frequency band and the resulting SPBW for each design. It is obtained a linear increase of the bandwidth as the order of the coupled SIW LWA increases; from 2.6% (400 MHz) for the N=1 antenna, to 6.4% (970 MHz) for the N=2b antenna, and finally to 9.5% (1420 MHz) for the N=3 SIW LWA design.

IV. EXPERIMENTAL VALIDATION

This section presents experimental results with manufactured prototypes of the designed antennas, which are shown in Fig.14.

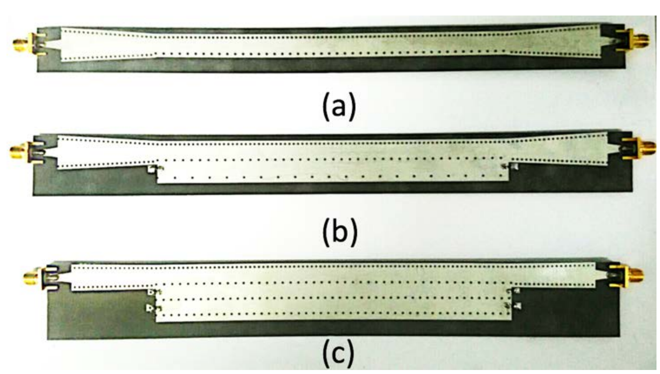

Fig. 14. Photograph of manufactured prototypes a) N=1 b) N=2b c) N=3.

All prototypes were manufactured using commercial RT-Duroid 5880 substrate (H=0.508mm, ε_r=2.2, tanδ=0.0009). As common in this type of SIW LWAs [4], [16] and also in general SIW circuits [34], [35], a width-tapered microstrip to SIW transition is used for improved matching [36], [37]. Both the microstrip and the closed SIW widths are linearly tapered, so that the mode conversion and matching is performed in two stages: first from the TEM mode of the 50Ω microstrip to the TE_{10} guided mode of the closed (non-leaky) SIW, and then from this guided TE_{10} mode to the quasi-TE_{10} leaky mode of the perturbed (leaky) SIW section. It must be taken into account that this type of SIW LWAs are more difficult to match than other SIW components as filters [35]-[37], since SIW LWAs operate close to the cutoff frequency of the SIW mode to make it leak. As a result, the width of the radiating leaky-SIW section is very narrow, and a width-tapered SIW transition from a wider guiding input section to this narrow radiating section is requested, as reported in [4], [16]. A detail of this feeding mechanism is illustrated in Fig.15 and the associated widths and lengths for each section are summarized in Table III.

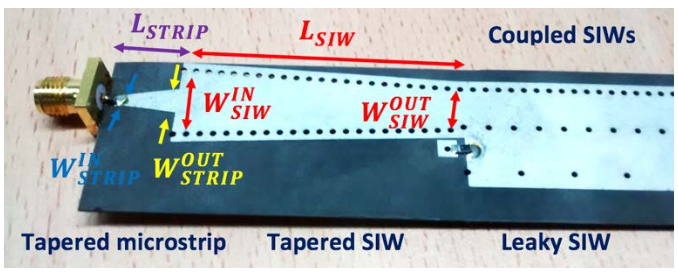

Fig. 15. Detail of microstrip-to-coupled-SIW leaky-line feeding.

TABLE III. MICROSTRIP-TO-LEAKY-SIW FEEDING

Parameter	Dimensions	Parameter	Dimensions
W^{IN}_{STRIP}	1.62 mm	W^{IN}_{SIW}	12.40 mm
W^{OUT}_{STRIP}	4.53 mm	W^{OUT}_{SIW}	7.40 mm
L_{STRIP}	10 mm	L_{SIW}	42 mm

The measured input matching for the three prototypes is plotted in Fig.16 together with simulated HFSS results, observing good agreement. The three coupled-SIW LWA prototypes present a cutoff frequency close to 14GHz, where the onset of the leaky-mode occurs radiating close to broadside direction (θ≈0º). As commented, it is difficult to match the structure at this cutoff frequency. Then, as frequency increases the matching improves showing a wide band with reduced S_{11}. The impedance-matching bandwidth with S_{11}<-10dB covers the range from 14.7GHz to 17GHz for the three designs.

However, the practical bandwidth of the antenna is limited by the aforementioned scanned pattern bandwidth (SPBW) for the desired scanning angle (in our case $\theta=\theta_{GOAL}$=30º). The simulated and measured frequency response of the gain at the designed scanning angle of θ_{GOAL}=30º for the three prototypes is reported in Fig.17.

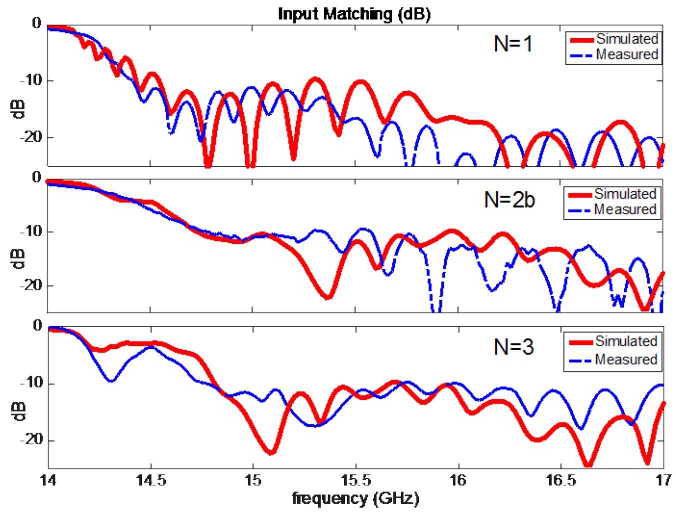

Fig. 16. Simulated and measured input matching frequency response for the three prototypes a) N=1 b) N=2b c) N=3.

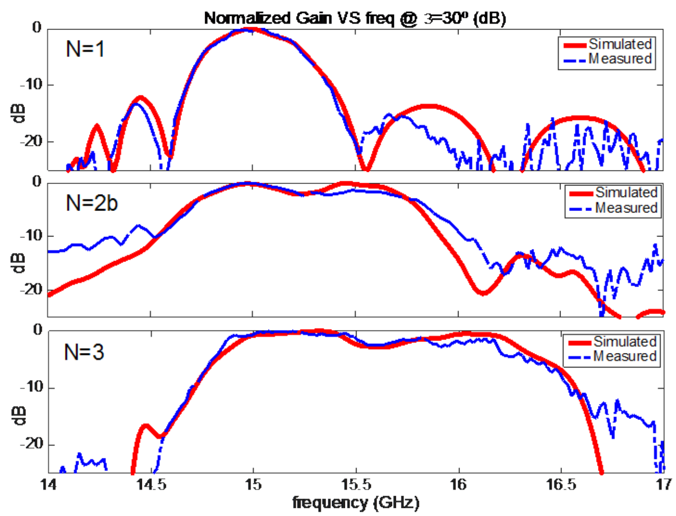

Fig. 17. Simulated and measured gain frequency response at the design scanned angle θ_{GOAL}=30º, for the three prototypes a) N=1 b) N=2b c) N=3.

Again, good agreement is observed in Fig.17 between simulations and experiments, demonstrating higher SPBW as the order of coupled SIWs is increased. Finally, Fig.18 compares the measured normalized gain frequency responses for the three manufactured prototypes, at the designed direction of θ=30º. Table IV summarizes the measured performance taking into account the two main limiting factors in the overall SIW antennas bandwidth: the input impedance bandwidth and the scanned pattern bandwidth for the scanning angle of θ=30º.

TABLE IV. ELECTROMAGNETIC PERFORMANCE OF PROTOTYPES

Case	Impedance Bandwidth (GHz) (S11<-10dB)	half-power gain bandwidth at θ=30º (GHz)	Peak Directivity (dBi)	Peak Gain (dBi)
N=1	14.42–17	14.82–15.20	13.9	12.8
N=2b	14.79–17	14.76–15.76	12.5	11.5
N=3	14.78–17	14.84–16.20	12.3	11.2

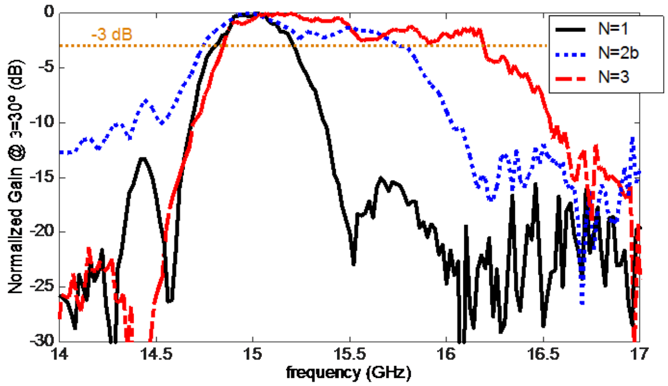

Fig. 18. Simulated and measured normalized gain vs. frequency response at scanned angle θ_{GOAL}=30º, for the three prototypes a) N=1 b) N=2b c) N=3.

The typical single-SIW LWA prototype shows a narrow gain bandwidth of 380MHz at 15GHz (i.e. 2.5% fractional SPBW), due to the well-known frequency beam squint associated to common SIW LWAs. The peak gain of this antenna is 12.8dBi, with an aperture length of L=16cm=8λ_0 at 15GHz, with a directivity of 13.9dBi and a radiation efficiency of 77.6%. The proposed new design with N=3 coupled SIWs demonstrate a superior performance, with a SPBW of 1360MHz and a peak gain of 11.2dBi (and similar radiation efficiency of 77.7% for a lower directivity of 12.3dBi). As usually happens, there is a tradeoff between gain and bandwidth. In our case this is translated into a 1.6dB drop in gain and directivity, for an improvement of 3.6 times of the associated pattern bandwidth (from 380MHz to 1360MHz, i.e. from 2.5% to 9% fractional bandwidth).

V. Conclusion

It has been demonstrated that by properly coupling leaky SIW lines, the beam-squint effect associated to directive scanned SIW LWAs can be reduced, obtaining a wider gain bandwidth for a designed elevation scanning angle. The proposed coupled-SIW LWA topology maintains the planar, single feeding, and passive properties of SIW LWAs. The structure is extremely integrated, thanks to the use of longitudinally coupled SIW guides along the antenna length. In this way, it is avoided the use of bulky 3D lenses, non-Foster active arrays, or more complicated nonreciprocal structures reported in previous squint-free LWAs technologies [6]-[15].

The design procedure is based on optimization of the reflection phase response of the coupled-cavity structure. Thanks to the use of analytical transverse-equivalent networks (TEN) based on leaky-mode dispersion theory, this optimization can be efficiently pursued if compared to previous wideband designs of coupled-cavity antennas [19]-[25], which rely on consuming full-wave simulations of the whole three-dimensional structure. The one-dimensional TEN allows simple yet accurate modelling of the multiple coupled-SIW-cavities and thus efficient design of the involved geometrical dimensions. This way, it has been demonstrated that the objective positive phase-gradient response can be achieved in a wider frequency band as the order of the coupled-SIW structure is increased. This has been demonstrated by optimizing N=2 and N=3 designs, which after the circuital optimization yield to reduced beam-squint effect at the desired scanning angle, as the number of coupled SIWs is increased. This translates into a novel anomalous oscillatory leaky-mode dispersion, which reports for the first time stabilization of the equivalent leaky-mode radiation angle around the desired scanning direction, over a wide frequency band. This simple modal study has been corroborated with the performance of the whole coupled-SIW antenna structure, which has shown increased half-power gain bandwidth of the simulated and measured gain at the designed scanning angle.

The measured results demonstrate the successful design of a third-order SIW LWA scanning at 30º with 11.2 dB gain and fractional pattern bandwidth of 9%. This is 3.6 times the bandwidth associated to a conventional LWA with similar aperture length based on a single leaky SIW, which presents 2.5% fractional pattern bandwidth at the same 30º direction and with 12.8 dB gain. The TEN used to design this wideband scanning SIW LWA, suggests that coupled-cavity filter synthesis techniques could be applied for a systematic design of this type of planar high-gain SIW antennas with application for broadband point-to-point wireless communications.

References

[1] A. A. Oliner and D. R. Jackson, “Leaky-wave antennas,” in *Antenna Engineering Handbook*, J. L. Volakis, Ed., 4th ed. New York: Mc- Graw-Hill, Jun. 2007, ch. 11.

[2] A. Sanada, H. Kubo, S.-I. Matsuzawa, and K. Sato, “Automotive radar antenna application using balanced composite right/left-handed metamaterials”, in *Proc. Antennas Propag. Soc. Int. Symp*., pp.398-401, Jul. 2006.

[3] M. Ettorre, A. Neto, G. Gerini, and S. Maci, “Leaky-wave slot array antenna fed by a dual reflector system,” *IEEE Trans. Antennas Propag.*, vol. 56, no. 10, pp. 3143–3149, Oct. 2008.

[4] Y. J. Cheng, W. Hong, K. Wu and Y. Fan, "Millimeter-Wave Substrate Integrated Waveguide Long Slot Leaky-Wave Antennas and Two-Dimensional Multibeam Applications," *IEEE Trans. Antennas Propag.*, vol. 59, no. 1, pp. 40-47, Jan. 2011.

[5] J.L. Gómez-Tornero, F.D. Quesada, A.A. Melcón, G. Goussetis, A.R. Weily, and Y. Jay Guo, "Frequency steerable two dimensional focusing using rectilinear leaky-wave lenses," *IEEE Trans. Antennas Propag.*, vol.59, no.2, pp. 407–415, Feb. 2011.

[6] A. Neto, S. Bruni, G. Gerini, and M. Sabbadini, “The leaky lens: A broad-band fixed-beam leaky-wave antenna,” *IEEE Trans. Antennas Propag.*, vol. 53, no. 10, pp. 3240–3246, Oct. 2005.

[7] A. Neto, "UWB, Non Dispersive Radiation From the Planarly Fed Leaky Lens Antenna— Part 1: Theory and Design," *IEEE Trans. Antennas Propag.*, vol. 58, no. 7, pp. 2238-2247, Jul. 2010.

[8] C. Caloz, S. Abielmona, H. Nguyen, and A.Rennings, “Dual composite right/left-handed (D-CRLH) leaky-wave antenna with low beam squinting and tunable group velocity”, *physica status solidi (b)*, vol. 244, no. 4, pp. 1219-1226, 2007.

[9] M. A. Antoniades, and G. V. Eleftheriades, “A CPS leaky-wave antenna with reduced beam squinting using NRI-TL metamaterials,” *IEEE Trans. Antennas Propag.*, vol. 56, no. 3, pp. 708–721, Mar. 2008.

[10] N. Nasimuddin, Z. N. Chen and X. Qing, "Substrate Integrated Metamaterial-Based Leaky-Wave Antenna With Improved Boresight Radiation Bandwidth," *IEEE Trans. Antennas Propag.*, vol. 61, no. 7, pp. 3451-3457, July 2013.

[11] K. M. Kossifos and M. A. Antoniades, "Analysis of an off-broadside zero beam-squinting leaky-wave antenna using metamaterials," *2016 18th*

Mediterranean Electrotechnical Conference (MELECON), Lemesos, Cyprus, 2016, pp. 1-4.

[12] A. Shahvarpour, A. Alvarez-Melcon, and C. Caloz, “Bandwidth enhancement and beam squint reduction of leaky modes in a uniaxially anisotropic meta-substrate,” in *Proc. Antennas Propag. Soc. Int. Symp*., pp. 1–4, Jul. 2010.

[13] A. Porokhnyuk, T. Ueda, Y. Kado, and T. Itoh, "Nonreciprocal metamaterial for non-squinting leaky-wave antenna with enhanced beam steering", in *Proc. Antennas Propag. Soc. Int. Symp*, pp. 2289 – 2290, Jul. 2013.

[14] D. F. Sievenpiper, “Superluminal waveguides based on non-foster circuits for broadband leaky-wave antennas”, *IEEE Antennas and Wireless Propagat. Lett*., vol.10, pp.231-234, 2011.

[15] D. Muha, S. Hrabar, I. Krois, I. Bonić, A. Kiričenko and D. Zaluški, "Design of microstrip non-foster leaky-wave antenna," in *21st International Conference on Applied Electromagnetics and Communications* (ICECom), Dubrovnik, pp. 1-3. 2013.

[16] A. J. Martinez-Ros, J. L. Gomez-Tornero, and G. Goussetis, “Planar leaky-wave antenna with flexible control of the complex propagation constant,” *IEEE Trans. Antennas Propag*., vol. 60, no. 3, pp. 1625-1630, Mar. 2012.

[17] J.L. Gómez-Tornero, A. Martínez-Ros, A. Álvarez-Melcón, F. Mesa and F. Medina, "Substrate integrated waveguide leaky-wave antenna with reduced beam squint," Microwave Conference (EuMC), 2013 European, Nuremberg, 2013, pp. 491-494.

[18] J.L. Gómez-Tornero, M. Poveda-García, R. Guzmán-Quirós, D. Cañete-Rebenaque, “Reducing the Beam Squint in Scanned Leaky-Wave Antennas using Coupled SIW Cavities”, in *Proc. Antennas Propag. Soc. Int. Symp*, pp. 77 – 78, Jul. 2016.

[19] A. P. Feresidis, J. C. Vardaxoglou, “A broadband high-gain resonant cavity antenna with single feed”, *Proc. EuCAP* 2006, Nice, France, 2006.

[20] M. A. Al-Tarifi, D. E. Anagnostou, A. K. Amert and K. W. Whites, "Bandwidth Enhancement of the Resonant Cavity Antenna by Using Two Dielectric Superstrates," *IEEE Trans. Antennas Propag*., vol. 61, no. 4, pp. 1898-1908, April 2013.

[21] C. Mateo-Segura, A.P. Feresidis, and G. Goussetis, "Bandwidth Enhancement of 2-D Leaky-Wave Antennas With Double-Layer Periodic Surfaces," *IEEE Trans. Antennas Propag.*, vol.62, no.2, pp. 586-593, Feb. 2014.

[22] K. Konstantinidis, A. P. Feresidis and P. S. Hall, "Multilayer Partially Reflective Surfaces for Broadband Fabry-Perot Cavity Antennas," *IEEE Trans. Antennas Propag.*, vol. 62, no. 7, pp. 3474-3481, July 2014.

[23] K. Konstantinidis, A. P. Feresidis and P. S. Hall, "Broadband Sub-Wavelength Profile High-Gain Antennas Based on Multi-Layer Metasurfaces," *IEEE Trans. Antennas Propag.*, vol. 63, no. 1, pp. 423-427, Jan. 2015.

[24] B. P. Chacko, G. Augustin and T. A. Denidni, "FPC Antennas : C-band point-to-point communication systems.," in *IEEE Antennas and Propagation Magazine*, vol. 58, no. 1, pp. 56-64, Feb. 2016.

[25] A. Chaabane, F. Djahli, H. Attia, L.M. Abdelghani, and T.A. Denidni, “Wideband and high-gain EBG resonator antenna based on dual layer PRS”, *Microw. Opt. Technol. Lett.*, vol.59, pp. 98–101, Jan. 2017.

[26] A. J. Martinez-Ros, J. L. Gomez-Tornero, and F. Quesada-Pereira, “Efficient analysis and design of novel SIW leaky-wave antenna,” *IEEE Antennas Wireless Propag. Lett.*, vol. 12, pp. 496–499, 2013.

[27] N. Marcuvitz, *Waveguide handbook*. P. Peregrinus on behalf of the Institution of Electrical Engineers, Ch.5, Sec.5-21, “Inductive posts”, pp. 285-289, 1986.

[28] E. Kuester, R. Johnk, and D. Chang, “The thin-substrate approximation for reflection from the end of a slab-loaded parallel-plate waveguide with application to microstrip patch antennas,” *IEEE Trans. Antennas Propag.*, vol. 30, no. 5, pp. 910 – 917, Sep. 1982.

[29] Ansoft HFSS Version 12.0 1984–2011, Ansoft Corporation.

[30] G. Yuehe, K.P. Esselle, and T.S. Bird, “The use of simple thin partially reflective surfaces with positive reflection phase gradients to design wideband, low-profile EBG resonator antennas”, *IEEE Trans. Antennas and Propag.*, vol. 60, no.2, pp. 743-750, Feb. 2012.

[31] B. A. Zeb, G. Yuehe, K.P. Esselle, Z. Sun, and M. E. Tobar, “A simple dual-band electromagnetic band gap resonator antenna based on inverted reflection phase gradient”, *IEEE Trans. Antennas and Propag.*, vol. 60, no.10, pp. 4522-4529, Oct. 2012.

[32] N. Wang, Q. Liu, C. Wu, L. Talbi, Q. Zeng and J. Xu, "Wideband Fabry-Perot Resonator Antenna With Two Complementary FSS Layers," in *IEEE Transactions on Antennas and Propagation*, vol. 62, no. 5, pp. 2463-2471, May 2014.

[33] A. Hosseini, F. Capolino and D. R. Jackson, "Leaky-wave explanation of gain-bandwidth-enhanced Fabry-Pérot Cavity antennas formed by a thick multilayer partially-reflective surface," in *Proc. Antennas Propag. Soc. Int. Symp*., Vancouver, BC, pp. 1090-1091, July 2015.

[34] D. Deslandes and K. Wu, “Integrated microstrip and rectangular waveguide in planar form,” *IEEE Microwave Wireless Comp. Lett.*, vol. 11, Feb. 2001.

[35] D. Deslandes and K. Wu, “Single-substrate integration technique of planar circuits and waveguide filters integrated microstrip and rectangular waveguide in planar form,” *IEEE Trans. Microwave Theory Tech.*, vol. 51, pp.338–339, Feb. 2003.

[36] D. Deslandes, “Design equations for tapered microstrip-to-substrate integrated waveguide transitions,” in *Proc. IEEE MTT–S Intern.Microwave Symp.*, May 2010, pp. 1–1.

[37] E. Miralles, H. Esteban, C. Bachiller, A. Belenguer, and V. E. Boria, “Improvement for the design equations for tapered microstrip–to–substrate integrated waveguide transitions,” in *Proc. Intern. Conf. Electromagnetics Adv. Appl.*, Sep. 2011, pp. 652–655.

[38] G. L. Matthaei, L. Young, and E. M. T. Jones, Microwave Filters, Impedance Matching Networks and Coupling Structures. New York: McGraw-Hill, 1965.